025921-27-T

Modeling of resistive sheets in finite element solutions

J. M. Jin, J. L. Volakis, C. L. Yu and A. C. Woo

National Aeronautics and Space Administration
Ames Research Center
Moffett Field CA 94035

Pacific Missile Test Center
Pt. Mugu CA
93042-5000

February 1992

THE UNIVERSITY OF MICHIGAN
Radiation Laboratory
Department of Electrical Engineering
and Computer Science
Ann Arbor, Michigan 48109-2122
USA

TECHNICAL REPORT

for NASA Grant NAG-2-541

NASA Technical Monitor: Alex Woo

Grant Title:	Development of 3D Electromagnetic Modeling Tools for Airborne Vehicles
Report Title:	Modeling of Resistive Sheets in Finite Element Solutions
Institution:	Radiation Laboratory Department of Electrical Engineering and Computer Science The University of Michigan Ann Arbor MI 48109-2122
Period Covered:	September 1991 – February 1992
Report Authors:	J.M. Jin and J.L. Volakis
Principal Investigator:	John L. Volakis Telephone: (313) 764-0500

Modeling of Resistive Sheets in Finite Element Solutions

J.M. Jin and J.L. Volakis
Radiation Laboratory
Department of Electrical Engineering and Computer Science
University of Michigan
Ann Arbor, MI 48109-2122

C.L. Yu
Pacific Missile Test Center
Pt. Mugu, CA 93042-5000
and
A.C. Woo
NASA-Ames Research Center
Moffett Field, CA 94035-1000

February 18, 1992

Abstract

A formulation is presented for modeling a resistive card in the context of the finite element method. The appropriate variational function is derived and for validation purposes results are presented for the scattering by a metal-backed cavity loaded with a resistive card.

1 Introduction

A resistive card is an infinitesimally thin sheet of material which allows partial penetration of the electromagnetic field. Thin dielectric layers and very thin conductors whose thickness is less than the skin depth are examples of materials which can be modelled by resistive cards or sheets. Resistive cards are often used for radar cross section and RF power penetration control and as a result they have been studied extensively. Such studies have generally been done in the context of high frequency [1], [2] and integral equation solutions [3], [4], but to date the treatment of resistive cards within the context of the finite element method (FEM) has not been considered. Over the past few years, FEM has been applied to a variety of electromagnetic problems and it is thus important to incorporate the modeling of resistive cards in the FEM. In this paper we propose an FEM formulation which accounts for the presence of resistive sheets. To validate this formulation, results based on a physical modeling of the resistive sheet are also presented. In this case, the resistive sheet is equivalently replaced by a thin dielectric layer. The modeling of such a layer in the usual manner leads to larger and consequently inefficient linear systems, which is the primary reason for resorting to a mathematical modeling of the resistive sheet. Results based on the mathematical and physical modeling are presented in connection with the scattering by a metal-backed cavity in a ground plane and these are used to validate the proposed mathematical model.

2 Formulation

A resistive sheet is characterized by its resistivity R which is measured in Ohms per square. Mathematically, it satisfies the boundary condition [5]

$$\hat{n}_r \times (\hat{n}_r \times \mathbf{E}) = -R\, \hat{n}_r \times \left(\mathbf{H}^+ - \mathbf{H}^-\right) \tag{1}$$

where $\mathbf{H}^{\pm}$ denotes the magnetic field above and below the sheet, $\mathbf{E}$ is the electric field and its tangential component is continuous across the sheet, and $\hat{n}_r$ denotes the unit vector normal to the sheet pointing in the upward direction (+ side). To a first order, this boundary condition can be used to simulate the presence of a thin dielectric layer by setting [4], [5]

$$R = \frac{Z_0}{jk_0\,(\tilde{\epsilon}_r - 1)\,t}. \tag{2}$$

In this, t is the thickness of the layer, Z_0 and k_0 denote the free space intrinsic impedance and wave number, respectively, and $\tilde{\epsilon}_r$ is the relative dielectric constant of the layer. Alternatively, a resistive sheet may be equivalently replaced by a thin dielectric layer having thickness t and a relative permittivity of

$$\tilde{\epsilon}_r = 1 - \frac{jZ_0}{k_0 t R}. \tag{3}$$

Generally, the accuracy of this simulation increases as the thickness t is decreased. Typically, t should not exceed one-tenth of the wavelength in the material.

Let us now consider a finite element solution of the fields within a volume V subject to a given excitation. The volume consists of some inhomogeneous dielectric having relative permittivity and permeability ϵ_r and μ_r, respectively, and we shall also assume that resistive cards may be embedded within the dielectric (see Figure 1). Within this volume, the electric field satisfies the vector wave equation

$$\nabla \times \left(\frac{1}{\mu_r}\nabla \times \mathbf{E}\right) - k_0^2 \epsilon_r \mathbf{E} = -jk_0 Z_0 \mathbf{J}^{\text{int}} + \nabla \times \left(\frac{1}{\mu_r}\mathbf{M}^{\text{int}}\right) \tag{4}$$

where $(\mathbf{J}^{\text{int}}, \mathbf{M}^{\text{int}})$ denote the impressed sources internal to the volume. Assuming a known tangential magnetic field on the boundary surface S_o enclosing V, the electric and magnetic fields must satisfy the relation

$$\hat{n}_o \times \nabla \times \mathbf{E} = -jk_0 Z_0 \mu_r \hat{n}_o \times \mathbf{H} \tag{5}$$

in which $\hat{n}_o$ is the outward unit vector normal to S_o. This is simply a statement of Maxwell's equations for the tangential boundary fields.

For a finite element solution of the subject field, we introduce the functional

$$\begin{aligned} F(\mathbf{E}) = \frac{1}{2} &\iiint_V \left[\frac{1}{\mu_r}(\nabla \times \mathbf{E}) \cdot (\nabla \times \mathbf{E}) - k_0^2 \epsilon_r \mathbf{E} \cdot \mathbf{E}\right] dV \\ &+ \iiint_V \mathbf{E} \cdot \left[jk_0 Z_0 \mathbf{J}^{\text{int}} - \nabla \times \left(\frac{1}{\mu_r}\mathbf{M}^{\text{int}}\right)\right] dV \\ &+ \frac{j}{2} k_0 Z_0 \iint_{S_r} \frac{1}{R}(\hat{n}_r \times \mathbf{E}) \cdot (\hat{n}_r \times \mathbf{E})\, dS \\ &+ jk_0 Z_0 \oiint_{S_o} \mathbf{E} \cdot (\mathbf{H} \times \hat{n}_o)\, dS \end{aligned} \tag{6}$$

in which S_r denotes the surface of the resistive sheet within V. We assert that F is stationary with respect to the true solution which satisfies (1), (4) and (5) and to prove this, we take the first variation of (6) with respect to $\mathbf{E}$ giving

$$\begin{aligned}\delta F = &\iiint_V \left[\frac{1}{\mu_r}(\nabla \times \mathbf{E}) \cdot (\nabla \times \delta\mathbf{E}) - k_0^2 \epsilon_r \mathbf{E} \cdot \delta\mathbf{E}\right] dV \\ &+ \iiint_V \delta\mathbf{E} \cdot \left[jk_0 Z_0 \mathbf{J}^{\text{int}} - \nabla \times \left(\frac{1}{\mu_r}\mathbf{M}^{\text{int}}\right)\right] dV \\ &+ jk_0 Z_0 \iint_{S_r} \frac{1}{R}(\hat{n}_r \times \mathbf{E}) \cdot (\hat{n}_r \times \delta\mathbf{E})\, dS \\ &+ jk_0 Z_0 \oiint_{S_o} \delta\mathbf{E} \cdot (\mathbf{H} \times \hat{n}_o)\, dS. \end{aligned} \tag{7}$$

On invoking a common vector identity, this can be rewritten as

$$\begin{aligned}\delta F = &\iiint_V \left[\nabla \times \left(\frac{1}{\mu_r}\nabla \times \mathbf{E}\right) - k_0^2 \epsilon_r \mathbf{E} + jk_0 Z_0 \mathbf{J}^{\text{int}} - \nabla \times \left(\frac{1}{\mu_r}\mathbf{M}^{\text{int}}\right)\right] \cdot \delta\mathbf{E}\, dV \\ &+ \iiint_V \nabla \cdot \left[\delta\mathbf{E} \times \left(\frac{1}{\mu_r}\nabla \times \mathbf{E}\right)\right] dV \\ &+ jk_0 Z_0 \iint_{S_r} \frac{1}{R}(\hat{n}_r \times \mathbf{E}) \cdot (\hat{n}_r \times \delta\mathbf{E})\, dS \\ &+ jk_0 Z_0 \oiint_{S_o} \delta\mathbf{E} \cdot (\mathbf{H} \times \hat{n}_o)\, dS \end{aligned} \tag{8}$$

where we can now employ the divergence theorem for the second integral. Doing so and noting that the tangential magnetic field on S_r is discontinuous we obtain

$$\begin{aligned}\delta F = &\iiint_V \left[\nabla \times \left(\frac{1}{\mu_r}\nabla \times \mathbf{E}\right) - k_0^2 \epsilon_r \mathbf{E} + jk_0 Z_0 \mathbf{J}^{\text{int}} - \nabla \times \left(\frac{1}{\mu_r}\mathbf{M}^{\text{int}}\right)\right] \cdot \delta\mathbf{E}\, dV \\ &+ \iint_{S_o + S_r^+ + S_r^-} \left[\delta\mathbf{E} \times \left(\frac{1}{\mu_r}\nabla \times \mathbf{E}\right)\right] \cdot \hat{n} dS \\ &+ jk_0 Z_0 \iint_{S_r} \frac{1}{R}(\hat{n}_r \times \mathbf{E}) \cdot (\hat{n}_r \times \delta\mathbf{E})\, dS \\ &+ jk_0 Z_0 \oiint_{S_o} \delta\mathbf{E} \cdot (\mathbf{H} \times \hat{n}_o)\, dS \end{aligned} \tag{9}$$

where S_r^+ denotes the top (or + side) surface of the resistive sheet and S_r^- denotes its bottom surface. Noting that $\hat{n}_r \times \mathbf{E}$ is continuous across S_r and that the

normals on S_r^+ and S_r^- are in opposite directions, it follows that

$$\delta F = \iiint_V \left[\nabla \times \left(\frac{1}{\mu_r}\nabla \times \mathbf{E}\right) - k_0^2 \epsilon_r \mathbf{E} + jk_0 Z_0 \mathbf{J}^{\text{int}} - \nabla \times \left(\frac{1}{\mu_r}\mathbf{M}^{\text{int}}\right)\right] \cdot \delta\mathbf{E}\, dV$$
$$-jk_0 Z_0 \iint_{S_r} \left[\frac{1}{R}\hat{n}_r \times (\hat{n}_r \times \mathbf{E}) + \hat{n}_r \times \left(\mathbf{H}^+ - \mathbf{H}^-\right)\right] \cdot \delta\mathbf{E}\, dS$$
$$- \oiint_{S_o} \left[\hat{n}_o \times \left(\frac{1}{\mu_r}\nabla \times \mathbf{E}\right) + jk_0 Z_0 \hat{n}_o \times \mathbf{H}\right] \cdot \delta\mathbf{E}\, dS. \qquad (10)$$

On invoking the conditions (1), (4) and (5), it is seen that $\delta F = 0$ proving our original premise that F is stationary with respect to the maxwellian field $\mathbf{E}$.

Having obtained the explicit form of the functional F, we may proceed to discretize it numerically in accordance with the finite element method by first subdividing the volume V into smaller volume elements and subsequently expanding the element field using vector basis functions. Substituting the field expansion into the functional and applying the Rayleigh-Ritz procedure (equivalent to setting the first variation of F to zero), we can obtain a system of equations involving the interior and boundary electric fields and the boundary magnetic fields. For a unique solution of this system we must, however, specify a relation between the tangential electric and magnetic field which appear in the surface integral over S_o. This can be provided by a boundary integral equation and the less accurate absorbing boundary conditions. If we assume the subject volume to be that occupied by the metal-backed cavity recessed in a ground plane, as shown in Figure 2, then S_o reduces to the aperture area of that cavity. By invoking image theory, the magnetic field on the aperture can then be expressed as

$$\mathbf{H} = \mathbf{H}^{\text{inc}} + \mathbf{H}^{\text{ref}} - 2jk_0 Y_0 \iint_{S_a} \left[\left(\bar{\mathbf{I}} + \frac{1}{k_0^2}\nabla\nabla\right) G_0(\mathbf{r}, \mathbf{r}')\right] \cdot [\mathbf{E}(\mathbf{r}) \times \hat{z}]\, dS' \qquad (11)$$

where S_a denotes the aperture surface, $G_0(\mathbf{r}, \mathbf{r}')$ is the free space scalar Green's function, $\mathbf{r}$ specifies the observation point located on S_a and $\bar{\mathbf{I}} = \hat{x}\hat{x} + \hat{y}\hat{y} + \hat{z}\hat{z}$ is the unit dyad. Also, $\mathbf{H}^{\text{inc}}$ denotes the magnetic field generated by sources in free space and $\mathbf{H}^{\text{ref}}$ is the corresponding reflected field when the cavity's aperture is shorted. A Galerkin's discretization of (11) yields a system relating the aperture electric and magnetic fields and when it is combined with the finite element system we can obtain a complete system for a unique solution of the interior and boundary fields. The system obtained in such a manner will be partly sparse

and partly full. In particular the volume integrals and that over S_r in (7) lead to a sparse submatrix involving the interior fields of the cavity. However, the discretization of (11) over S_a renders a full Toeplitz submatrix since the boundary integral is convolutional. Consequently, by resorting to an iterative solution such as the conjugate or biconjugate gradient method in conjunction with the fast Fourier transform, the need to generate the Toeplitz matrix is eliminated thus maintaining the $O(N)$ storage requirement, characteristic of finite element solutions. The details pertaining to this implementation are discussed in [6]-[8]. In the next section we only present some results aimed at evaluating the accuracy of the proposed resistive sheet model.

3 Numerical Results

Let us consider the metal-backed rectangular cavity illustrated in Figure 2. The cavity is assumed to be empty (no internal sources) and is illuminated by a plane wave in the $\phi = 0$ plane. To implement the aforementioned solution, the cavity is subdivided into rectangular bricks and the results of the solution are shown in Figure 3. These are radar cross section (RCS) patterns and refer to a 1λ deep cavity whose aperture is also $1\lambda \times 1\lambda$. The RCS pattern in Figure 3(b) applies to the cavity which is loaded with a resistive sheet of $100\Omega/\square$ placed at its aperture, whereas the result in Figure 3(a) is for the untreated empty cavity. The simulation of the resistive sheet was done through direct discretization of the first variation of the functional F as given in (6) and alternatively by modeling the resistive sheet as a dielectric layer of thickness $\lambda/20$ having the dielectric constant computed from (3). As shown in Figure 3(b) the results based on the two simulations are in reasonable agreement and the differences among them is due to the finite thickness which was necessarily introduced in the physical model of the resistive sheet. To support this statement, in Figure 4 we show the RCS computed at $\theta = 40°$ for several different thicknesses of the dielectric layer. The RCS value corresponding to the ideal resistive sheet simulation coincides with $t = 0$ of the plot. As seen, for smaller t the physical simulation is in better agreement with the ideal resistive sheet simulation. When $t = \lambda/20$, one can expect a difference of one to two dB between the physical and mathematical simulation.

The second geometry which was considered is a circular metal-backed cavity again situated in a ground plane. In this case the aperture of the circular cavity

is loaded with a sheet having non-uniform resistivity given by

$$R(\rho) = \begin{cases} Z_0 \left[0.1 + 10\left(\frac{a-\rho}{a}\right)^2\right] & \rho > 0.5a \\ \infty & \text{elsewhere on } S_a \end{cases} \tag{12}$$

where a denotes the radius of the aperture. Results with and without resistive loading for a cavity having $a = 1$ in. and a depth of 0.25 in. are shown in Figure 5. These RCS patterns were computed at 16GHz and the incident field was a plane wave polarized along the θ or ϕ directions. Again, the data in Figure 5 demonstrate the validity of the proposed mathematical model. Also, as in the case of the rectangular cavity the presence of the resistive cards reduces the overall RCS of the cavity and this reduction is primarily due to the reduced field intensity near its perimeter.

4 Conclusions

A variational formulation was presented for modeling resistive cards within the context of the finite element method. Results based on the discretization of the variational expression were also presented and these were aimed at demonstrating the validity and accuracy of the proposed mathematical model. Modeling of conductive sheets [5] can be accomplished by employing the magnetic field formulation yielding a functional which is the dual of (6). However, when the conductive and resistive sheets are both present within the computational domain one cannot avoid the introduction of double nodes on both sides of the surface occupied by the conductive or resistive sheets. If an electric field formulation is employed as given here, double nodes must be placed on the surface of the conductive sheet. The functional in (6) must also be supplemented with the additional integral

$$\frac{j}{2} k_0 Z_0 \iint_{S_c} R_m \left[\hat{n}_c \times (\mathbf{E}^+ - \mathbf{E}^-)\right] \cdot \left[\hat{n}_c \times (\mathbf{E}^+ - \mathbf{E}^-)\right] \, dS \tag{13}$$

where S_c is the surface occupied by the conductive sheet, R_m denotes its conductivity and $\hat{n}_c$ is the normal to the sheet. Other than the requirement to introduce double nodes on S_c, the implementation of (13) is straightforward.

References

[1] T.B.A. Senior, "Scattering by Resistive Strips," *Radio Science*, Vol. **14**, pp. 911-924, 1979.

[2] M.I. Herman and J.L. Volakis, "High Frequency Scattering by a Resistive Strip and Extensions to Conductive and Impedance Strips," *Radio Science*, Vol. **22**, pp. 335-349, May-June 1987.

[3] E.F. Knott and T.B.A. Senior, "Non-Specular Radar Cross Section Study," University of Michigan Radiation Laboratory Technical Report 011764-1-T (also U.S. Air Force Avionics Lab. report AFAL-TR-73-422) January 1974.

[4] R.F. Harrington and J.R. Mautz, "An Impedance Sheet Approximation for Thin Dielectric Shells," *IEEE Trans. Antennas Propagat.*, Vol. **AP-23**, pp. 531-534, 1975.

[5] T.B.A. Senior, "Combined Resistive and Conductive Sheets," *IEEE Trans. Antennas Propagat.*, Vol. **AP-33**, pp. 577-579, 1985.

[6] J.M. Jin and J.L. Volakis, "A Finite Element-Boundary Integral Formulation for Scattering by Three-Dimensional Cavity-Backed Apertures," *IEEE Trans. Antennas Propagat.*, Vol. **AP-39**, pp. 97-104, January 1991.

[7] J.M. Jin and J.L. Volakis, "Electromagnetic Scattering by and Transmission Through a Three-Dimensional Slot in a Thick Conducting Plane," *IEEE Trans. Antennas Propagat.*, Vol. **AP-39**, pp. 543-550, April 1991.

[8] J.M. Jin and J.L. Volakis, "A Hybrid Finite Element Method for Scattering and Radiation by Microstrip Patch Antennas and Arrays Residing in a Cavity," *IEEE Trans. Antennas Propagat.*, Vol. **AP-39**, pp. 1598-1604, Nov. 1991.

FIGURE CAPTIONS

Fig. 1 Cross section of a dielectric volume enclosing a resistive card.

Fig. 2 Geometry of a cavity-backed aperture in a ground plane.

Fig. 3 Monostatic RCS for a square aperture ($1\lambda \times 1\lambda$) backed by a rectangular cavity ($1\lambda \times 1\lambda \times 1\lambda$) in the $\phi = 0$ plane. (a) Empty cavity without resistive loading. (b) Empty cavity whose aperture is covered with a resistive sheet of a resistivity of 100 $\Omega/\square$. (Solid and dashed lines correspond to results based on the mathematical simulation; circles and squares refer to results based on the physical modeling of the resistive sheet).

Fig. 4 Monostatic RCS at $(\theta = 40^o, \phi = 0)$ of the square aperture in Fig. 3(b) as a function of the laryer thickness simulating the resistive sheet at the aperture. The $\tilde{\epsilon}_r$ of the layer is given by (3) with $R = 100\Omega/\square$.

Fig. 5 Monostatic RCS for a circular aperture (1 inch in diameter) backed by a circular cavity (1 inch in diameter and 0.25 inch in depth) at 16 GHz. (a) Empty cavity without resistive loading. (b) Empty cavity covered with a resistive sheet whose resistivity is given by (12). (Solid and dashed lines correspond to results based on the mathematical simulation; circles and squares refer to results based on the physical modeling of the resistive sheet).

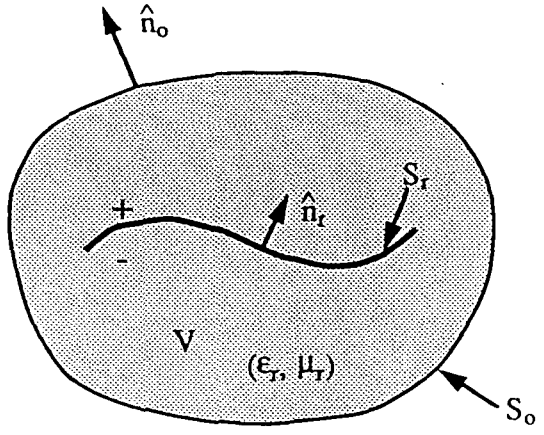

Fig. 1.

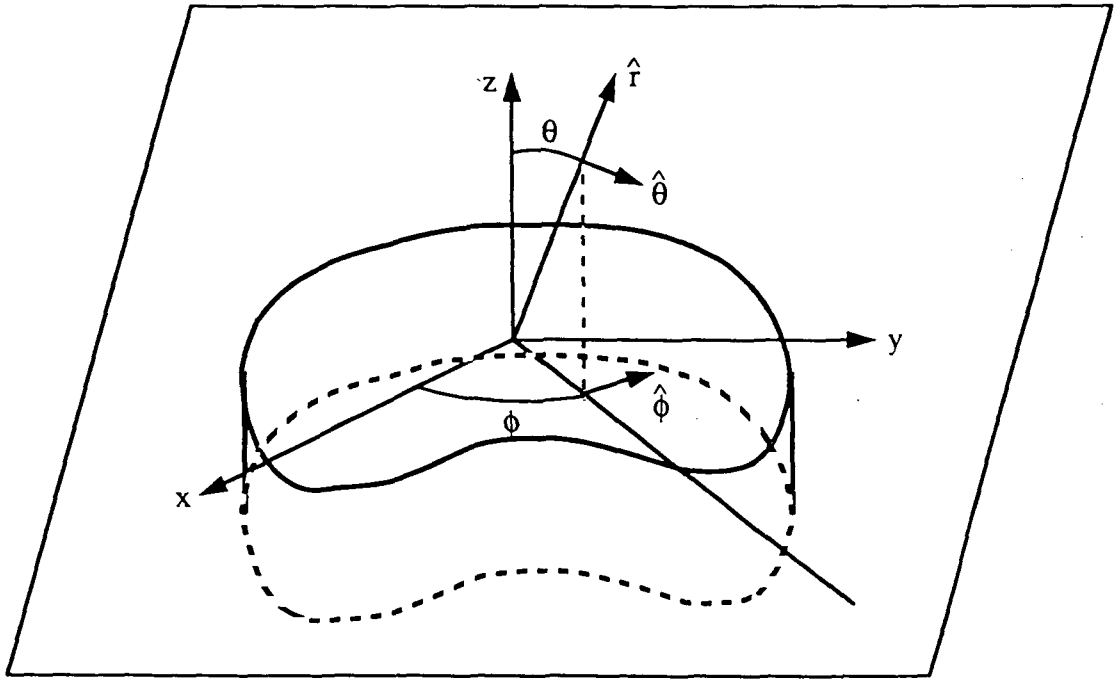

Figure 2

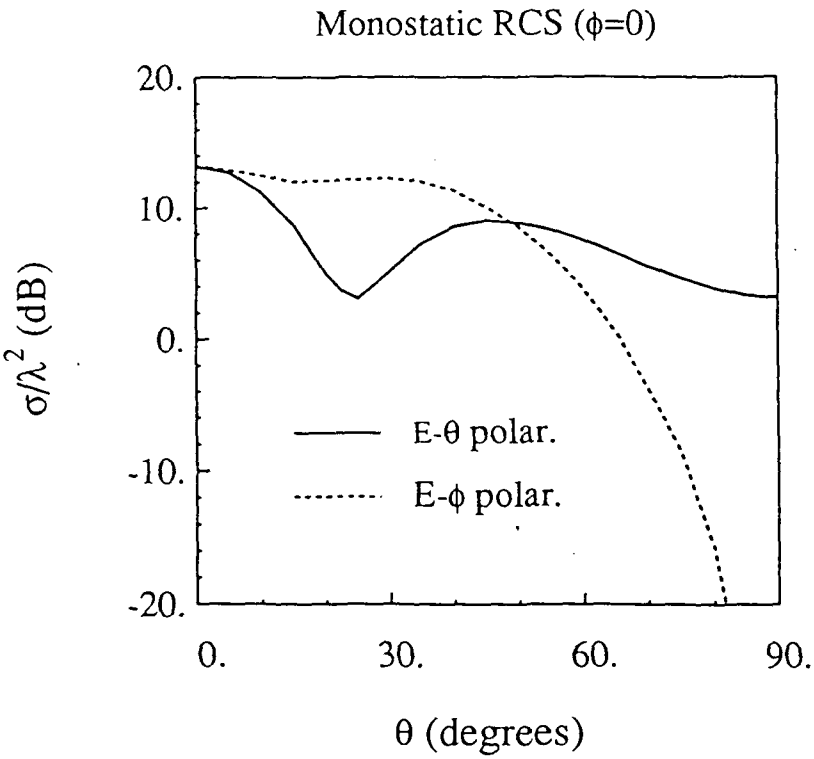
Monostatic RCS (ϕ=0)
20.
10.
0.
-10.
-20.
σ/λ² (dB)
E-θ polar.
E-ϕ polar.
0.
30.
60.
90.
θ (degrees)

Fig. 3(a)

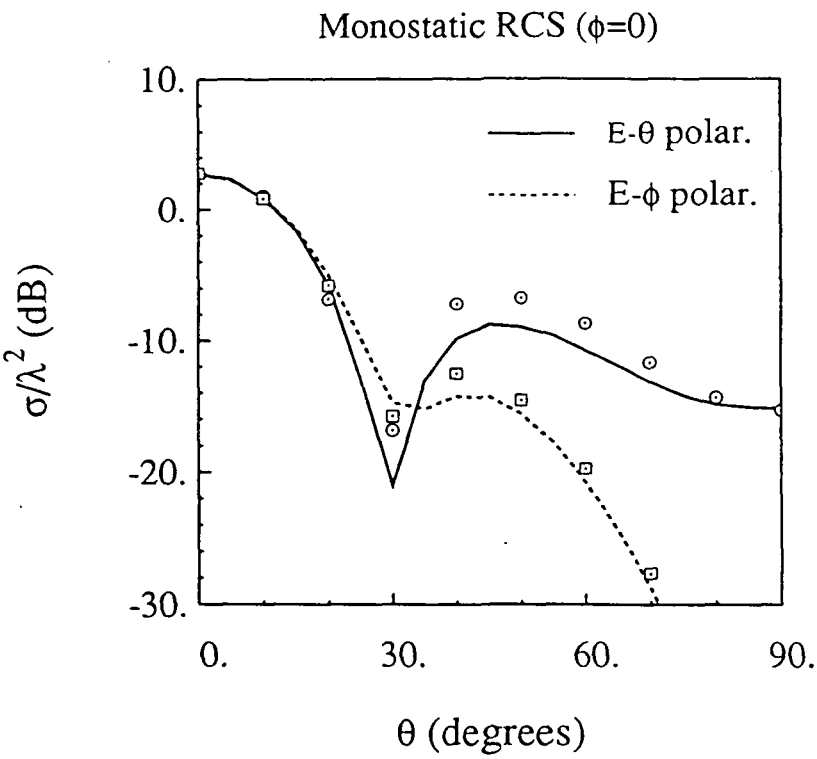
Monostatic RCS (ϕ=0)
10.
0.
-10.
-20.
-30.
0.
30.
60.
90.
σ/λ² (dB)
θ (degrees)
E-θ polar.
E-ϕ polar.

Fig. 3(b)

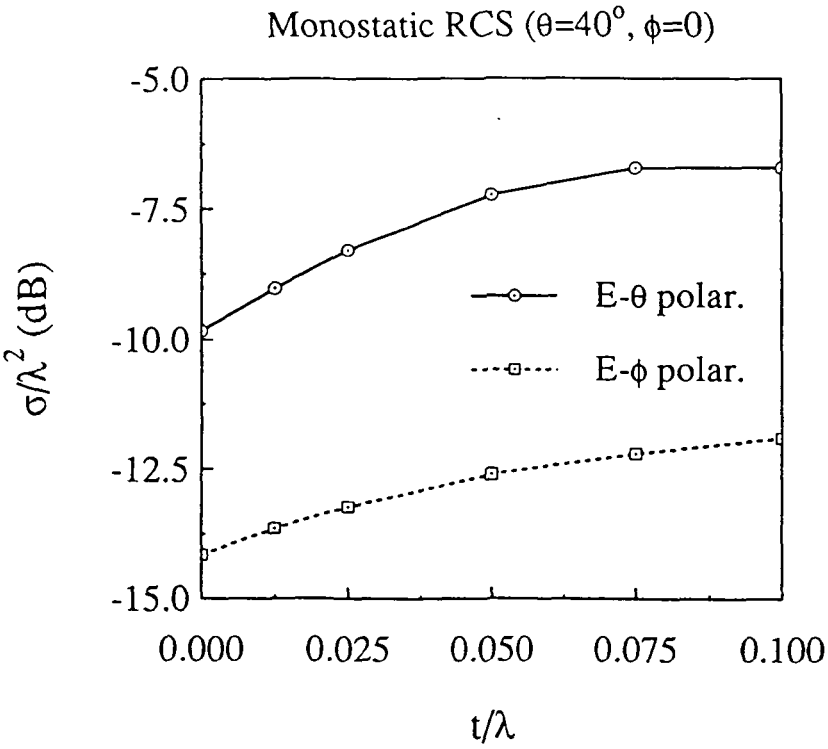
Monostatic RCS (θ=40°, ϕ=0)
-5.0
-7.5
-10.0
-12.5
-15.0
σ/λ² (dB)
E-θ polar.
E-ϕ polar.
0.000
0.025
0.050
0.075
0.100
t/λ

Fig. 4

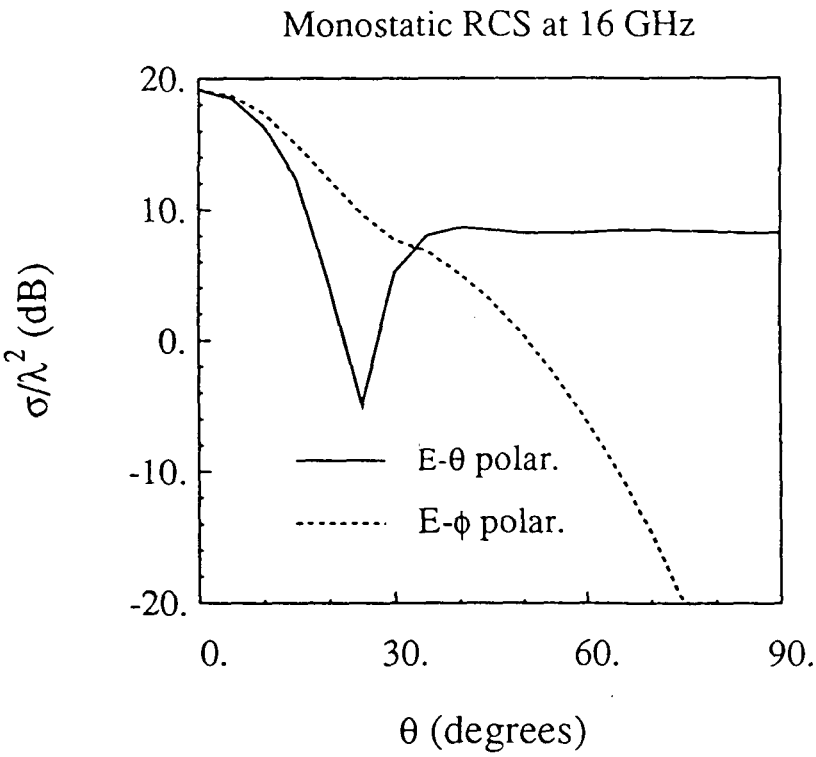
Monostatic RCS at 16 GHz
20.
10.
0.
-10.
-20.
σ/λ² (dB)
E-θ polar.
E-ϕ polar.
0.
30.
60.
90.
θ (degrees)

Fig. 5(a)

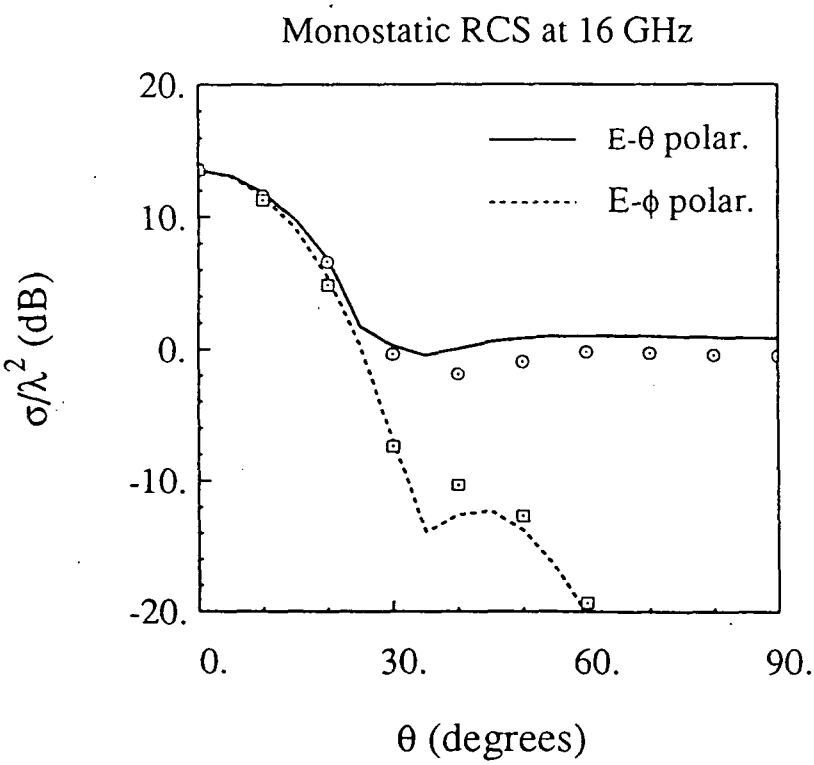
Monostatic RCS at 16 GHz
20.
10.
0.
-10.
-20.
0.
30.
60.
90.
σ/λ² (dB)
θ (degrees)
E-θ polar.
E-ϕ polar.

Fig. 5(b)